ACCURATE ORIENTATION ESTIMATION FOR SEISMIC SENSORS UNDER ENVIRONMENTAL MAGNETIC DISTURBANCES

Yadongyang ZHU[1], Bo LAN[1], Fang WANG[1], Wenhao WEI[2]*

A common problem limiting data analysis in seismic exploration is the determination of sensor orientation. To solve this problem, we developed an orientation estimation method for seismic sensors using an attitude measurement system. Heading angle is usually obtained by combining gyroscope and magnetometer measurements, but in real-world environments ferromagnetic objects will cause disturbances in the magnetic field, leading to significant errors in estimated heading angles. Therefore, in this paper we propose a method of detecting magnetic disturbances that is calibrated using the unscented Kalman filter (UKF). The proposed technique can be used in online detection and implemented in inexpensive, small-scale microprocessors and sensor modules. First, magnetic disturbances are detected by exploiting variations in the magnetic strength and magnetic dip angle. Second, the relationship between the magnetometer error values at adjacent times is described so that a compensation model can be derived. Finally, the correction method is based on the UKF. Moreover, the estimated heading angle is able to be quickly restored to its normal value once the magnetic disturbance disappears. The proposed method was tested in an indoor environment with various magnetic disturbances, and we designed a rotating platform for conducting tests. In the case with magnetic disturbances, the proposed method could correct the heading angle, whether in regular or irregular motion. The output precision could be controlled to within 2°. The proposed method can be used in several systems, e.g., vertical seismic profilers, free-fall ocean bottom seismometers, and deep towed acoustic and geophysical systems.

Keywords: Seismic sensors, Orientation estimation, Magnetic disturbance, Sensor fusion, Kalman filter

1. Introduction

The orientations of the three components of seismic sensors (geophones, seismometers, or hydrophones) are always uncontrollable and random in seismic exploration. For example, in vertical seismic profiling (VSP) acquisition, the orientation of horizontal elements cannot be controlled by Sonde cables for current borehole systems [1]. In deploying free-fall ocean bottom seismometers

[1] School of Information Engineering, Beijing Institute of Petrochemical Technology, China
[2] North Automatic Control Technique Research Institute, Taiyuan 030006, China
∗ Corresponding author: Wenhao Wei, e-mail: 398314449@qq.com

(OBS), the main difficulty is that users do not have complete control over how and where the station lands [2]. Regarding the positions of the hydrophones in relation to the tow fish in the Deep Towed Acoustic/Geophysical System (DTAGS), the geometry of acquisition changes with every action of the winch, since any displacement of the seismic source affects streamer shape [3].

Therefore, because of this, the first step in data processing is determination of the orientations of the seismic sensors [4], the usual method of which is application of geophysical methods to retrieve the relative orientation based on post-processing of the signals. The azimuthal orientations of geophones in a vertical well were determined by Di Siena et al. with a maximum-energy solution during VSP data processing [1]. To determine a probe's orientation in an inclined well, a polarization analysis method was used by Beque [5]. Cross-correlation was implemented by Zeng and McMechan to discover the angles between adjacent geophones [6], while a complex linear least squares method was used by Grigoli et al. to obtain this same information [7]. Zhu et al. developed a least squares method based on quaternions to obtain the relative rotation between geophone pairs [8]. One can apply similar techniques, e.g., using artificial reference signals [9], polarization analysis [10], or cross-correlation analysis [11] to determine the orientations of OBS sensors. To determine absolute orientation, however, these techniques unfortunately usually require prior knowledge of either a seismic reference sensor or the location of a known source.

The addition of an attitude sensor to measure geophone orientations is another solution. A seismic sensor's orientation can be measured using an accelerometer and a gyroscope [12,13], which sometimes provides a higher degree of accuracy. Using a gyroscope for long periods of time reduces measurement accuracy through the introduction of a cumulative error [14]. Hundreds of sensors are needed in seismic exploration, but the use of high-precision gyroscopes in such deployments dramatically increases production costs. A drilling tool's orientation in an oil well is normally measured with an accelerometer and magnetometer [15,16], but magnetometers are susceptible to changes in the environmental magnetic field. Therefore, in the event of magnetic disturbances, the accuracy of the measured orientation using both instruments is significantly affected [17,18].

Owing to the aforementioned reasons, we propose a method in this paper that estimates seismic sensor orientations through an attitude measurement system consisting of gyroscopes, accelerometers, and magnetometers. In practical applications, determining the orientations from different measuring sensors is an example of data fusion. Thus, the extended Kalman filter (EKF) integrates the values measured by three separate sensors from the AHRS. In real-world environments, however, ferromagnetic objects will disturb the magnetic field and induce serious errors in estimated heading angles [23]. In this study, magnetic

disturbances were detected by exploiting variations in the magnetic strength and the magnetic dip angle, and a method was proposed to compensate for magnetic disturbances based on the unscented Kalman filter (UKF). The algorithm used was evaluated under static and dynamic laboratory conditions. The results showed that the proposed algorithm achieved errors of less than 2° in the presence of various magnetic disturbances.

2. Orientation Estimation Method

2.1. Model definition

An AHRS comprises either microelectromechanical or solid-state system gyroscopes, magnetometers, and accelerometers, and the sensor fusion method employed can provide orientation information such as roll, pitch, and yaw. The AHRS used in the present study was the XSENS MTI-1, the dimensions of which are 12.1× 12.1×2.55 mm3. Compared with a discrete design, its structure is simple, easy to install, and inexpensive. Moreover, it corrects the errors of the three types of attitude sensors before delivery, obviating the need for complex calibration in use; only a simple command set is used to obtain more accurate measurement output [19,20].

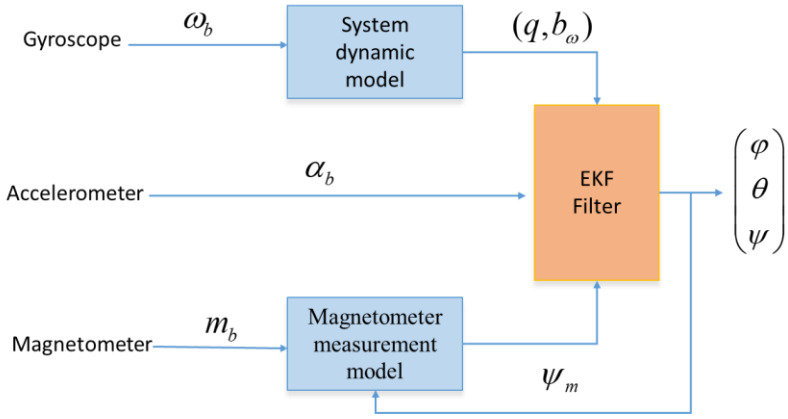

Fig. 1 Schematic of the extended Kalman filter (EKF)

The data fusion algorithm in this paper adopts the EKF [22], and the schematic of the EKF is shown in Fig. 1.

The nonlinear state-space model is

$$\mathrm{x}(k) = f(x(k-1), k-1) + w(k-1) \tag{1}$$

$$\mathrm{z}(k) = h(x(k), k) + v(k) \tag{2}$$

where $x(k) \in R^n$ is the state vector at time k, $z(k) \in R^m$ is the measurement vector at time k, f(·) is a real n vector function, and h(·) is a real m vector function. f(·) and h(·) are nonlinear with respect to their independent variables. $w(k) \in R^n$ and $v(k) \in R^m$ are the process noise vector with the covariances $Q(k)$ and $R(k)$, respectively.

The system state is assumed to be the following:

$$x(k) = (q_0(k) \quad q_1(k) \quad q_2(k) \quad q_3(k) \quad b_{\omega x}(k) \quad b_{\omega y}(k) \quad b_{\omega z}(k)) \tag{3}$$

where $q_0(k), q_1(k), q_2(k), q_3(k)$ are the attitude quaternions, and $b_{\omega x}(k), b_{\omega y}(k), b_{\omega z}(k)$ are the random drift vectors of the gyroscope.

The state equation is as follows:

$$x(k) = \begin{pmatrix} q(k) \\ b_w(k) \end{pmatrix} = \begin{pmatrix} (I + (T/2)\Omega_w) q_{k-1} \\ b_w(k-1) \end{pmatrix} + \begin{pmatrix} w_q(k-1) \\ w_w(k-1) \end{pmatrix} = f(x(k-1), k\text{-}1) \tag{4}$$

The Jacobi matrix for $f(x(k-1), k-1)$ is defined as follows:

$$\Phi(k, k-1) = \left. \frac{\partial f(x(k-1), k-1)}{\partial x(k-1)} \right|_{x(k-1)=\hat{x}(k-1)} \tag{5}$$

where $(\hat{\omega}_x, \hat{\omega}_y, \hat{\omega}_z)^T = (\omega_x, \omega_y, \omega_z)^T - (b_{\omega x}, b_{\omega y}, b_{\omega z})^T$, $\hat{\omega}_x, \hat{\omega}_y, \hat{\omega}_z$ are the predicted values for the gyroscope, and $\omega_x, \omega_y, \omega_z$ are the measured values for the gyroscope.

The process noise covariance matrix $Q(k)$ is as follows:

$$Q(k) = \begin{bmatrix} \sigma_q^2 I_{4\times 4} & 0 \\ 0 & \sigma_\omega^2 I_{3\times 3} \end{bmatrix} \tag{6}$$

The measurement state is assumed to be the following:

$$z(k) = (a_{bx}(k), a_{by}(k), a_{bz}(k), \varphi_m(k))^T \tag{7}$$

where $a_{bx}(k)$, $a_{by}(k)$, $a_{bz}(k)$ are the measurements from the triaxial accelerometer, and $\varphi_m(k)$ is the projection of the magnetometer measurement on a horizontal plane.

$a_{bx}(k)$, $a_{by}(k)$, $a_{bz}(k)$, and g have the following relationships:

$$\begin{pmatrix} a_{bx} \\ a_{by} \\ a_{bz} \end{pmatrix} = c_n^b \begin{pmatrix} 0 \\ 0 \\ -g \end{pmatrix} = \begin{pmatrix} -2g(q_1q_3 - q_0q_2) \\ -2g(q_2q_3 + q_0q_1) \\ -2(q_0^2 - q_1^2 - q_2^2 + q_3^2) \end{pmatrix} \tag{8}$$

The measurement equation is as follows:

$$z(k) = \begin{pmatrix} a_{bx}(k) \\ a_{by}(k) \\ a_{bz}(k) \\ \varphi_m(k) \end{pmatrix} = \begin{pmatrix} -2g(q_1q_3 - q_0q_2) \\ -2g(q_2q_3 + q_0q_1) \\ -2(q_0^2 - q_1^2 - q_2^2 + q_3^2) \\ \arctan\left(-\dfrac{2(q_1q_2 - q_0q_3)}{q_0^2 - q_1^2 + q_2^2 - q_3^2}\right) \end{pmatrix} + v(k) = h(x(k),k) + v(k) \tag{9}$$

The Jacobi matrix for $h(x(k),k)$ is computed as follows:

$$H(k) = \left.\frac{\partial H(x(k),k)}{\partial x(k)}\right|_{x(k)=\hat{x}(k,k-1)} \tag{10}$$

The measurement noise covariance matrix $R(k)$ is as follows:

$$R(k) = \begin{bmatrix} \sigma_a^2 I_{3\times3} & 0 \\ 0 & \sigma_m^2 I_{1\times1} \end{bmatrix} \tag{11}$$

2.2 Extended Kalman filter (EKF) Implementation

The optimal estimation of the system's state vector is obtained iteratively through the derived state equation and the measurement equation. The EKF recursive process proceeds as follows.

1) Initialization:

The initial value of the state $x(0)$, process noise covariance matrix $Q(k)$, measurement noise covariance matrix $R(k)$, and error covariance matrix $P(0)$ are set.

2) Prediction:

The Jacobi matrix for $f(x(k-1),k-1)$ is obtained:

$$\Phi(k,k-1) = \left.\frac{\partial f(x(k-1),k-1)}{\partial x(k-1)}\right|_{x(k-1)=\hat{x}(k-1)} \tag{12}$$

The filter estimates the current state based on all the previous states:

$$\hat{x}(k,k-1) = f(\hat{x}(k-1),k-1) \tag{13}$$

Then, the a priori error covariance matrix is estimated based on the previous error covariance matrix, which is defined as follows:

$$P(k,k-1)=\Phi(k,k-1)P(k,k-1)\Phi^{T}(k,k-1)+Q(k) \tag{14}$$

3) Update:

The Jacobi matrix for $H(x(k),k)$ is obtained as follows:

$$H(k)=\left.\frac{\partial H(x(k),k)}{\partial x(k)}\right|_{x(k)=\hat{x}(k,k-1)} \tag{15}$$

The Kalman gain is calculated as follows:

$$K(k)=P(k,k-1)H^{T}(k)[(H(k)P(k,k-1)H^{T}(k)+R(k)]^{-1} \tag{16}$$

The state estimate is updated as follows:

$$\hat{x}(k)=\hat{x}(k,k-1)+K(k)[z(k)-h(\hat{x}(k,k-1),k)] \tag{17}$$

The error covariance is updated as follows:

$$P(k)=[I-K(k)H(k)]P(k,k-1)[I-K(k)H(k)]^{T}+K(k)R(k)K^{T}(k) \tag{18}$$

Through the above Kalman filtering process, the quaternion is recursively updated, and the attitude angle is finally solved. The formula is as follows:

$$\begin{pmatrix}\varphi\\ \theta\\ \phi\end{pmatrix}=\begin{pmatrix}-\arctan(2(q_1q_3+q_0q_2)/(q^2{}_0-q^2{}_1-q^2{}_2+q^2{}_3))\\ \arcsin(2(q_2q_3-q_0q_1))\\ -\arctan(2(q_1q_2+q_0q_3)/(q^2{}_0-q^2{}_1+q^2{}_2-q^2{}_3))\end{pmatrix} \tag{19}$$

3. Compensation for magnetic disturbance

3.1 Magnetic Disturbance

In practical applications, the AHRS mounted in the seismic sensors updates the heading angle with the Earth's ambient magnetic field and gravity vectors as reference vectors. If, however, the magnetic field is disturbed by nearby ferromagnetic materials, e.g., iron or steel, significant errors in estimated heading angle will result.

To detect a disturbance in the magnetic field, the magnetic dip angle and the total magnetic flux can be monitored. The magnetic dip angle, also known as the magnetic inclination, varies depending on the position of the Earth's surface; it is 0° at the magnetic equator and 90° at the two magnetic poles.

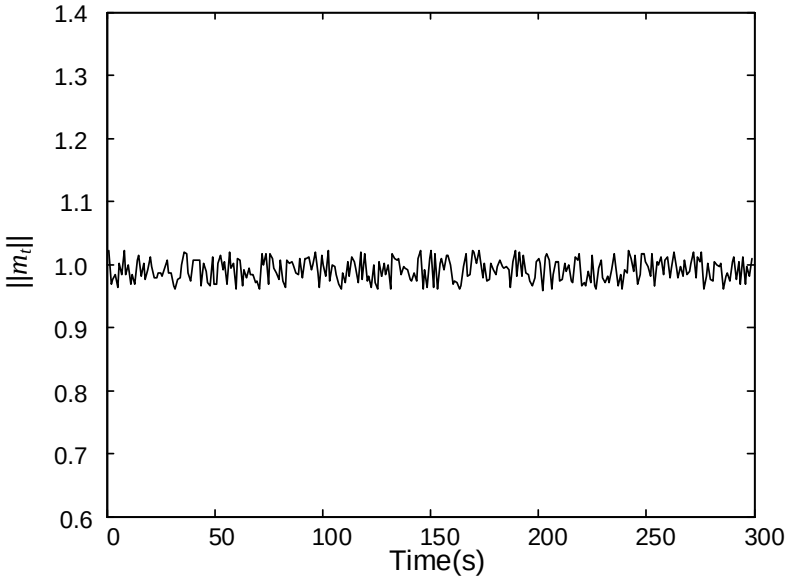

Fig. 2 Normalized strength of magnetic flux density with no magnetic disturbances

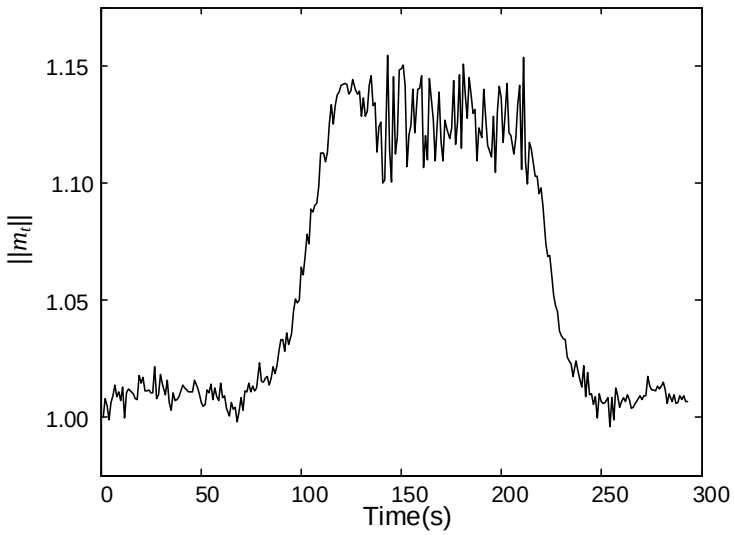

Fig. 3 Normalized strength of magnetic flux density with magnetic disturbances

The total flux $\|m_t\|$ can be calculated from the output values of the magnetometer's three components:

$$\|m_t\| = \sqrt{m_x^{\,2} + m_y^{\,2} + m_z^{\,2}} \tag{20}$$

To calculate the magnetic dip angle, the magnetometer's output should be expressed in the global frame as follows:

$$m^G = C_b^n \times [m_x, m_y, m_z]^T \tag{21}$$

The magnetic dip angle in the global frame is

$$\varphi_{mag} = \arctan\left(\frac{m_z^G}{\sqrt{(m_x^G)^2 + (m_y^G)^2 + (m_z^G)^2}}\right) \tag{22}$$

The magnetic dip angle and the total magnetic flux should remain constant if there is no magnetic disturbance. Fig. 2. shows the normalized strength of magnetic flux density with no magnetic disturbances. And Fig. 3. Shows the normalized strength of magnetic flux density with magnetic disturbances.

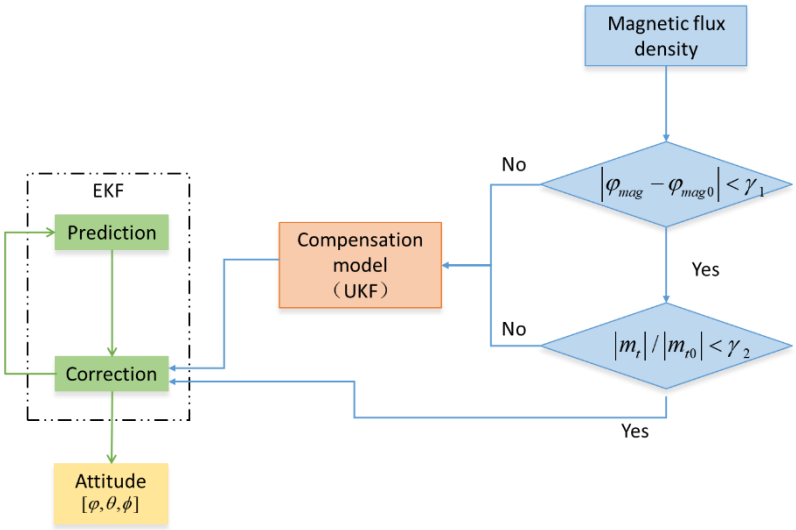

Fig. 4 Block diagram of the algorithm to detect a magnetic disturbance

The flow chart of the algorithm to detect the magnetic disturbances is shown in Fig. 4. The algorithm reads the output of the magnetometer. It monitors the magnetic dip angle and the total magnetic flux to determine whether the environmental magnetic disturbance has caused any abnormal changes. If both parameters are within their thresholds, the seismic sensors can be considered to not be near a magnetic disturbance.

To determine the thresholds, we conducted several tests. First, we measured the magnetometer's output while moving the magnetometer mounted on a seismic instrument following a straight path with no magnetic disturbances present. Second, we calculated the magnetic dip angles and the total magnetic flux. We then adjusted and verified the thresholds. The threshold should be evaluated and adjusted when necessary.

3.2 Compensation Model

When the magnetic disturbances were detected, the unscented Kalman filter (UKF) was used for calibration. For a magnetic disturbance detected at time t, the state equation is

$$X_t = A \bullet X_{t-1} + w_t \tag{23}$$

where the state vector is $X = \left[\Delta\theta, \Delta\varphi, \Delta\phi, d_x, d_y, d_z\right]^T$, which includes the change of the attitude angle $\Delta\alpha_t = [\Delta\theta, \Delta\varphi, \Delta\phi]$ and the magnetometer's error vector $d_t = [d_x, d_y, d_z]$, w_t is the process noise vector, and A is the state matrix.

The relationship between magnetometer error values at adjacent times is as follows:

$$d_t = c_d d_{t-1} + v_t \tag{24}$$

where c_d is a constant between 0 and 1, and v_t is the driving Gaussian noise.

To facilitate the operation, new variables are introduced as follows:

$$\begin{bmatrix} d_{bx} \\ d_{by} \\ d_{bz} \end{bmatrix} = C_n^b \begin{bmatrix} d_x \\ d_y \\ d_z \end{bmatrix} \tag{25}$$

According to the formulas above, we can derive the following:

$$\begin{cases} \Delta\alpha_t = c_\alpha \Delta\alpha_{t-1} + v_{v_t} \\ C_{n(t)}^b d_t = c_\alpha C_{n(t-1)}^b d_t + v_{m_t} \end{cases} \tag{26}$$

That is,

$$\begin{cases} \Delta\alpha_t = c_\alpha \Delta\alpha_{t-1} + v_{v_t} \\ d_t = c_\alpha (C_{n(t)}^b)^{-1} C_{n(t-1)}^b d_t + v_{m_t} \end{cases} \tag{27}$$

where c_α is a constant between 0 and 1, v_{v_t} is the attitude error matrix, and v_{m_t} is the magnetic disturbance error matrix. Both matrices are Gaussian noise matrices. The state equation is as follows:

$$X_t = A \bullet X_{t-1} + w_t = \begin{pmatrix} c_\alpha \Delta\alpha_{t-1} + v_{v_t} \\ c_\alpha (C_{n(t)}^b)^{-1} \bullet C_{n(t-1)}^b d_t + v_{m_t} \end{pmatrix} \tag{28}$$

The measurement equation is as follows [24]:

$$z_t = Z \bullet X_t + r_t \tag{29}$$

where z_t is the measurement value, Z is the measurement matrix, and r_t is the process noise vector.

The following formula is applied [21]:

$$\dot{C}_n^b = C_n^b [w_{RB}\times] \tag{30}$$

where $[w_{RB}\times]$ is as follows:

$$[w_{RB}\times] = \begin{bmatrix} 0 & -w_z & w_y \\ w_z & 0 & -w_x \\ -w_y & w_x & 0 \end{bmatrix} \tag{31}$$

Equation (30) can be written as follows:

$$\frac{C_{n(t)}^b - C_{n(t-1)}^b}{\Delta t} = C_{n(t-1)}^b [w_{RB}\times] \tag{32}$$

Moreover,

$$[w_{RB}\times]\times\Delta t = [\Delta\alpha] = \begin{bmatrix} 0 & -\Delta\phi & \Delta\varphi \\ \Delta\phi & 0 & -\Delta\theta \\ -\Delta\varphi & \Delta\theta & 0 \end{bmatrix} \tag{33}$$

Thus,

$$C_{n(t)}^b = C_{n(t-1)}^b \begin{bmatrix} 1 & -\Delta\phi & \Delta\varphi \\ \Delta\phi & 1 & -\Delta\theta \\ -\Delta\varphi & \Delta\theta & 1 \end{bmatrix} \tag{34}$$

Both sides of the equation are multiplied by $\begin{bmatrix} M\cos\eta & 0 & M\sin\eta \end{bmatrix}^T$, and it is rewritten as follows:

$$M_{(t)} = C_{n(t-1)}^b \begin{bmatrix} 1 & -\Delta\phi & \Delta\varphi \\ \Delta\phi & 1 & -\Delta\theta \\ -\Delta\varphi & \Delta\theta & 1 \end{bmatrix} \begin{bmatrix} M\cos\eta \\ 0 \\ M\sin\eta \end{bmatrix} \tag{35}$$

When a magnetic disturbance is present, it can be expressed as follows:

$$M_{(t)} = C_{n(t-1)}^{b} \begin{bmatrix} 1 & -\Delta\phi & \Delta\varphi \\ \Delta\phi & 1 & -\Delta\theta \\ -\Delta\varphi & \Delta\theta & 1 \end{bmatrix} C_{n(t-1)}^{b\ -1} \bar{M}_{(t-1)} + \begin{bmatrix} d_{bx} \\ d_{by} \\ d_{bz} \end{bmatrix} \tag{36}$$

where $M_{(t)}$ is the magnetometer's output at time t, and $\bar{M}_{(t-1)}$ is the calibration value at time t−1. The measurement equation is as follows:

$$z_t = C_{n(t-1)}^{b} \begin{bmatrix} 1 & -\Delta\phi & \Delta\varphi \\ \Delta\phi & 1 & -\Delta\theta \\ -\Delta\varphi & \Delta\theta & 1 \end{bmatrix} C_{n(t-1)}^{b\ -1} \bar{M}_{(t-1)} + \begin{bmatrix} d_{bx} \\ d_{by} \\ d_{bz} \end{bmatrix} \tag{37}$$

By the above derivation, the model to calibrate the magnetometer based on the UKF is as follows:

$$\begin{cases} X_t = A \bullet X_{t-1} + w_t = \begin{pmatrix} c_\alpha \Delta\alpha_{t-1} + v_{v_t} \\ c_\alpha (C_{n(t)}^{b})^{-1} \bullet C_{n(t-1)}^{b} d_t + v_{m_t} \end{pmatrix} \\ z_t = C_{n(t-1)}^{b} \begin{bmatrix} 1 & -\Delta\phi & \Delta\varphi \\ \Delta\phi & 1 & -\Delta\theta \\ -\Delta\varphi & \Delta\theta & 1 \end{bmatrix} C_{n(t-1)}^{b\ -1} \bar{M}_{(t-1)} + \begin{bmatrix} d_{bx} \\ d_{by} \\ d_{bz} \end{bmatrix} \end{cases} \tag{38}$$

4. Tests and Analysis

4.1. Magnetic Disturbance Detection

To verify the compensation method for the magnetic disturbance, we designed a rotating platform for testing. The rotating platform could be freely rotated 360° around the X-, Y-, and Z-axes to meet the requirements of the experiment. The rotating platform is shown in Fig. 5. For seismic sensors (geophones, seismometers, or hydrophones), because of the cable traction, there would not be a large change in the attitude angle in a short time. Therefore, when the rotating platform was used for the rotation simulation, the simulation was carried out at relatively low speeds.

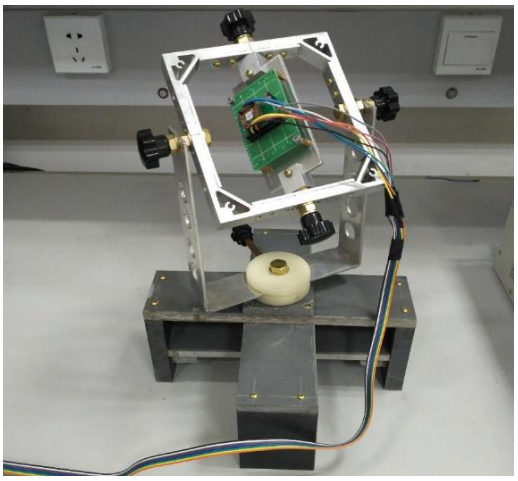

Fig. 5 Rotating platform

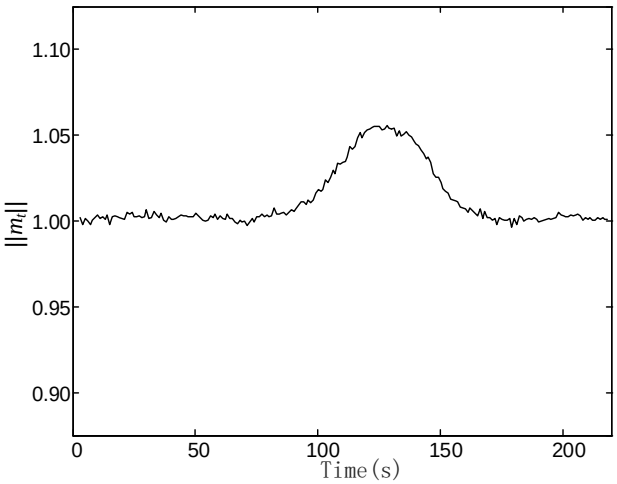

Fig. 6 Normalized strength of magnetic flux density of magnetic disturbances in test

To verify the detection algorithm of geomagnetic anomalies, a magnet was used to simulate magnetic disturbances in the laboratory environment. First, after the magnetometer was working properly, a period was waited. The magnet was then allowed to slowly approach the magnetometer and then gradually move away from it after a certain distance. Based on the output value of the magnetometer, the total flux was calculated. The results are shown in Fig. 6. The values changed significantly between 100 and 160 s, which could be judged to be abnormal measured values output by the magnetometer during this period. In other periods, the values were close to a constant value, and the magnetometer could be considered to have been in a normal working state during these periods.

4.2 Compensation Experiments

To verify the calibration method based on the UKF when a magnetic disturbance was detected, we conducted several groups of experiments. The experiments were all based on a rotating platform. The AHRS was fixed on the rotating platform while the experiment was carried out. During the experiment, the motion process of the carrier was simulated by the rotation of three axes. Magnets were used to simulate the occurrence of a magnetic disturbance, and the strength was simulated by adjusting the distance between the magnets and the AHRS. Because the magnetic disturbance only affected the azimuth, the simulation experiment was also conducted for the measurement of the azimuth.

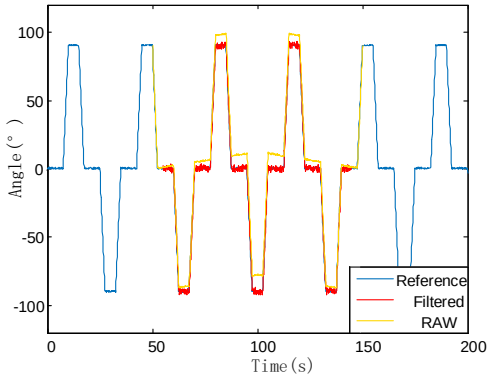

Fig. 7 Regular motion test

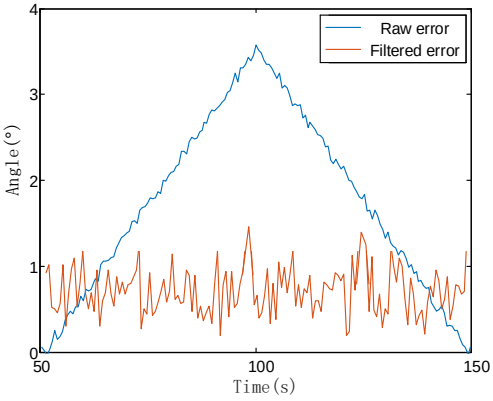

Fig. 8 Regular motion test error

In the first experiment, the AHRS performed a 90° azimuth rotation, and the magnet moved in a uniform straight line through a rotating platform. The data fusion of the three sensors in the AHRS was carried out by the EKF. During the experiment, the rotating platform rotated ±90° at the fixed point. At 50 s, the magnet started moving from the side of the rotating platform and moved in line across the rotating platform area. Fig. 7 shows the calculated azimuth angle. The blue line represents the theoretical value, the yellow line is the result of data fusion without magnetic calibration, and the red line is the result of the data fusion after magnetic calibration.

In the second experiment, the azimuth of the AHRS was rotated randomly, and the magnet moved randomly within the magnetic disturbance range. During the experiment, the azimuth of the rotating platform was rotated in an irregular way, and the magnet moved in an irregular way on the side of the rotating platform, forming an irregular magnetic disturbance. Fig. 9 shows the calculated azimuth angle. Black represents the theoretical value, blue represents the data fusion value without magnetometer calibration, and red represents data fusion value after magnetometer calibration. Through observation, it was found that the

results of the modified algorithm were better than the results of the unmodified algorithm after the magnetic disturbance appeared at 170 s.

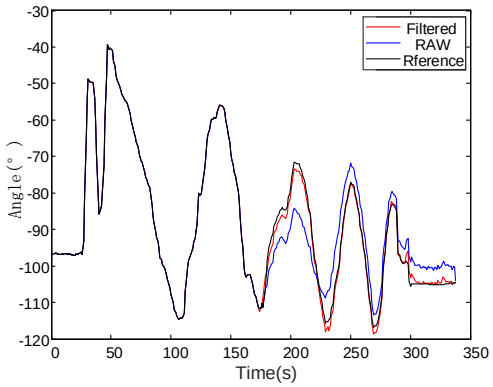

Fig. 9 Irregular motion test

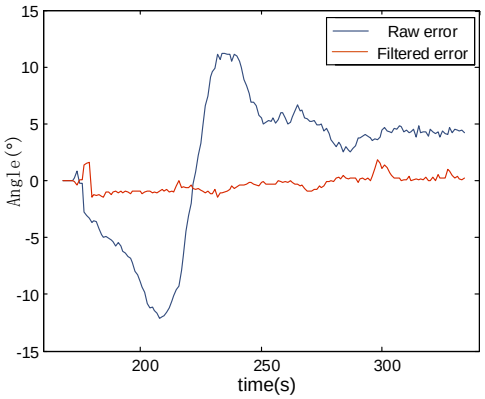

Fig. 10 Irregular motion test error

Fig. 10 shows the error curve obtained based on the calculation results in Fig. 9. The blue line represents the error between the uncalibrated results and the theoretical value, which changed with the change of the magnetic disturbance. The red line represents the error between the calibrated results and the theoretical value, which was basically stable within the range of 2°. The sudden change of the error was due to the sudden change of the angle during the irregular motion, but the overall situation was stable.

From the above two experiments, it can be concluded that in the case of a magnetic disturbance, whether in regular or irregular motion, the correction algorithm in this paper can be applied to correct the output azimuth angle, and the output precision can be controlled to within 2°.

5. Conclusion

In this paper, we developed an accurate orientation estimation for seismic instruments under environmental magnetic disturbances. The experimental results show that the output precision could be controlled to within 2° and demonstrate our method's validity and the system's feasibility. Compared with the traditional algorithm, our method can realize online detection, use the least number of sensors, and cost less. In our future works, we will consider the following aspects: 1) Although the UKF method we applied has achieved good results, it needs to be iterative, which makes our method unfriendly to the low-power MCU (Microcontroller Unit). We will try to design a solution method that can perform operations directly. 2) We have accumulated some measurement data under environmental magnetic disturbances in experiments. We will try to train some artificial neural networks to correct abnormal situations through the model. We

can even consider training an end-to-end artificial neural network model, which can complete anomaly detection and numerical compensation through one model.

Acknowledgments

This work was supported by the Natural Science Foundation of China (grant no. 42104175); General Project of Science and Technology Plan of Beijing Municipal Education Commission (grant no. KM202010017011); Cross-Disciplinary Science Foundation from Beijing Institute of Petrochemical Technology (project no. BIPTCSF-009).

R E F E R E N C E S

[1] *J. P. Di Siena, J. E. Gaiser, D. Corrigan.* Horizontal components and shear wave analysis of three component VSP data [J]. in Vertical Seismic Profiling, Part B: Advanced Concepts, 1984: 175-235.

[2] *T. Dahm, M. Thorwart, E. R. Flueh, et al.* Ocean Bottom Seismometers deployed in Tyrrhenian Sea [J]. Eos Transactions American Geophysical Union, 2013, 83(29): 309-315.

[3] *B. Marsset, E. Menut, S. Ker, et al.* Deep-towed High Resolution multichannel seismic imaging [J]. Deep-Sea Research Part I, 2014, 93: 83-90.

[4] *S. A. Greenhalgh, I. M. Mason.* Orientation of a downhole triaxial geophone [J]. GEOPHYSICS, 1995, 60(4): 1234-1237.

[5] *M. Becquey, M. Dubesset.* Three-component sonde orientation in a deviated well [J]. GEOPHYSICS, 1990, 55(10): 1386-1388.

[6] *X. Zeng, G. A. McMechan.* Two methods for determining geophone orientations from VSP data [J]. GEOPHYSICS, 2006, 71(4): V87-V97.

[7] *F. Grigoli, S. Cesca, T. Dahm, et al.* A complex linear least-squares method to derive relative and absolute orientations of seismic sensors[J]. Geophysical Journal International, 2012, 188(3): 1243-1254.

[8] *Y. Zhu, J. Lin, F. Zhao, et al.* A least squares method based on quaternions to derive absolute orientation of geophones with AHRS[J]. Journal of Geophysics and Engineering, 2018, (6): 6.

[9] *Y. Nakamura, Donoho, P.L., Roper, P.H. & McPherson, P.M.,.* Large offset seismic surveying using ocean-bottom seismographs and air gun: instrumentation and field technique [J]. GEOPHYSICS, 1987, 52(12): 1601-1611.

[10] *X.-Y. Li, J. Yuan.* Geophone orientation and coupling in three-component sea-floor data: a case study [J]. Geophysical Prospecting, 1999, 47(6): 995-1013.

[11] *M. Hensch.* On the interrelation of fluid-induced seismicity and crustal deformation at the Columbo submarine volcano (Aegean Sea, Greece) [J]. PhD thesis, 2009, University of Hamburg, Hamburg.:

[12] *R. Li, F. Li.* Accuracy improvements of gyro-based measurement-while-drilling surveying instruments by a laser testing method[J]. International Symposium on Photoelectronic Detection and Imaging, 2009, 7382: 8.

[13] *A. S. Jurkov, J. Cloutier, E. Pecht, et al.* Experimental Feasibility of the In-Drilling Alignment Method for Inertial Navigation in Measurement-While-Drilling [J]. IEEE Transactions on Instrumentation and Measurement, 2011, 60(3): 1080-1090.

[14] *Aboelmagd, N., Tabler, H., Irvine-Halliday, D. & Mintchev, M.P*., Quantitative Study of the Applicability of Fiber-Optic Gyroscopes for MWD Borehole Surveying, in SPE conference, 2000, pp. 363-370.

[15] *W. S. Luo, T. Xu, L. B. Du.* Directional drilling attitude measurement and azimuth correction with accelerometers and magnetometers [J]. Journal of National University of Defense Technology, 2007, 29: 106-110.

[16] *Y. Ren, Y. Wang, M. Wang, et al.* A Measuring System for Well Logging Attitude and a Method of Sensor Calibration [J]. sensors, 2014, 14(5): 9256.

[17] *N. Yadav, C. Bleakley.* Accurate Orientation Estimation Using AHRS under Conditions of Magnetic Distortion [J]. Sensors (Basel, Switzerland), 2014, 14(11):

[18] *J. Lee, J. Lim, J. Lee.* Compensated Heading Angles for Outdoor Mobile Robots in Magnetically Disturbed Environments [J]. IEEE Transactions on Industrial Electronics, 2017: 1-1.

[19] *D. Gebre-Egziabher, R. C. Hayward, J. D. Powell.* A low-cost GPS/inertial attitude heading reference system (AHRS) for general aviation applications[C]. Position Location and Navigation Symposium, IEEE, 2002, 518-525.

[20] *G. A. Song, Q. H. Zeng, B. Zhang, et al.* Design and Realization of Strapdown AHRS Based on DSP & CPLD [J]. Computer Technology & Development, 2012:

[21] *J. H. Espina-Hernández, R. Grössinger.* A pulse field magnetometer for local magnetization measurements [J]. Journal of Alloys & Compounds, 2004, 369(1): 235-238.

[22] *X. Geng et al.,* Carrier Dynamic Attitude Estimation Algorithm Based on MEMS Inertial Sensor [C]. IEEE the 2nd international conference on micro/nano sensors for ai, healthcare, and robotics (nsens), 2019, pp. 103-107.

[23] *Ye, F., Shi, F., Lai, Y. et al.* Heading angle estimation using rotating magnetometer for mobile robots under environmental magnetic disturbances [J]. Intel Serv Robotics, 2020, 13, 459–477.

[24] *Wu, J., Wang, X., Xiao, Q. et al.* Temperature correction method of sensor measured texture depth index based on equivalent temperature of asphalt surface layer [J]. Int. J. Pavement Res. Technol., 2021, 14, 450–458.